In situ azimuthal rotation device for linear dichroism measurements in scanning transmission x-ray microscopy

D. Hernández-Cruz and A. P. Hitchcock[a)]
Department of Chemistry and BIMR, McMaster University, Hamilton ON L8S 4M1, Canada

T. Tyliszczak
Advanced Light Source, LBNL, Berkeley California 94720

M.-E. Rousseau and M. Pézolet
Département de Chimie et CERSIM, Université Laval, Québec QC G1K 7P4, Canada

(Received 15 November 2006; accepted 21 February 2007; published online 26 March 2007)

A novel miniature rotation device used in conjunction with a scanning transmission x-ray microscope is described. It provides convenient *in situ* sample rotation to enable measurements of linear dichroism at high spatial resolution. The design, fabrication, and mechanical characterization are presented. This device has been used to generate quantitative maps of the spatial distribution of the orientation of proteins in several different spider and silkworm silks. Specifically, quantitative maps of the dichroic signal at the C $1s \rightarrow \pi^*_{\text{amide}}$ transition in longitudinal sections of the silk fibers give information about the spatial orientation, degree of alignment, and spatial distribution of protein peptide bonds. A new approach for analyzing the dichroic signal to extract orientation distributions, in addition to magnitudes of aligned components, is presented and illustrated with results from *Nephila clavipes* dragline spider silk measured using the *in situ* rotation device. © *2007 American Institute of Physics.* [DOI: 10.1063/1.2716502]

I. INTRODUCTION

Scanning transmission x-ray microscopy[1,2] (STXM) is a relatively new analytical microscopy technique used to study a wide diversity of materials, such as polymers, nanomaterials, extraterrestrial samples, biological, and environmental samples. Its powerful analytical capabilities are related to the details of near edge x-ray absorption spectra (NEXAFS). For oriented samples, the intensity of the NEXAFS spectra depends on the relative orientation of the electric vector (*E* vector) of the x-ray beam and the orientation of the transition moments associated with the absorption bands.[3] Quantitative measurements of this linear dichroic signal can be a useful complement to the NEXAFS spectrum when studying physical properties of anisotropic organic or inorganic materials. For example, the magnitude and angular variation of the linear dichroism provides information on the degree of crystallization and molecular orientation of the region of the sample under investigation. To probe this linear dichroic signal and thereby learn about the orientational properties of a sample, it is necessary to vary either the direction of the *E* vector of the light or to vary the orientation of the sample relative to a fixed *E* vector direction. The analysis of the orientation dependence of the NEXAFS spectra allows the identification of both the direction and magnitude of the dichroic signal, which in turn can be interpreted in terms of structure. The novel aspect of performing such measurements in STXM is that the spatial distribution of orientation can be measured quantitatively at a spatial resolution better than 50 nm. The first example of such an application of STXM was reported by Ade *et al.*[4,5] Recently, we have reported STXM linear dichroism studies of *Bombyx mori (B. mori)* cocoon silk[6] and *Nephila clavipes (N. clavipes)* spider silk.[7] The real-space orientation maps derived from spatially resolved dichroism signals measured with STXM complement earlier studies of the structure of silk by x-ray[8–10] and electron[11] diffraction techniques. The details of the comparison are left to other publications.

At the Advanced Light Source (ALS, Berkeley, California), there are two STXM instruments. The source of x-rays used in the STXM at beamline 11.0.2 (Ref. 12) is an Apple-2 type elliptically polarization undulator (EPU). For this STXM, the direction of the *E* vector of the linearly polarized light can be changed continuously from horizontal to vertical, over a range of 90°, by modifying the phase angle and gap of the EPU.[13] This control of the light polarization allows measurements of in-plane linear dichroic signals from samples without requiring azimuthal sample rotation. The second STXM, at ALS beamline 5.3.2,[14] is situated on a bend magnet port[15] which can only provide partially polarized light with a fixed horizontal polarization. Since the polarization direction is fixed, it is necessary to rotate the sample azimuthally and measure spectra at different angles to probe in-plane linear dichroism when using STXM 5.3.2. A sample holder which provides for manual azimuthal rotation (Fig. 1) has been used at ALS STXM 5.3.2 for some years. This is very tedious to use since changing the rotation angle requires opening the microscope, removing and rotating the sample, relocating the same area under an optical microscope, reinserting the sample into the STXM, reestab-

a)Electronic mail: aph@mcmaster.ca

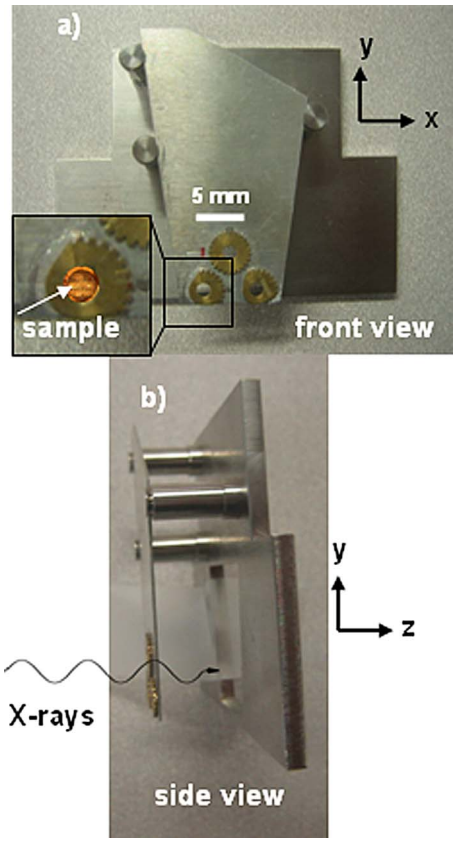

FIG. 1. The manual azimuthal rotation sample holder. It is displayed while being held in a three-pin kinematic mount, identical to that used in the STXM. (a) Front view. Inset shows a 3 mm copper grid (as used for transmission electron microscopy), mounted for measurements. (b) Side view.

lishing of the microscope conditions, and finding the same region of the sample to measure the next point of a dichroic curve. Typically, one manual angle change would take at least 30 min, whereas the measurement at any given angle

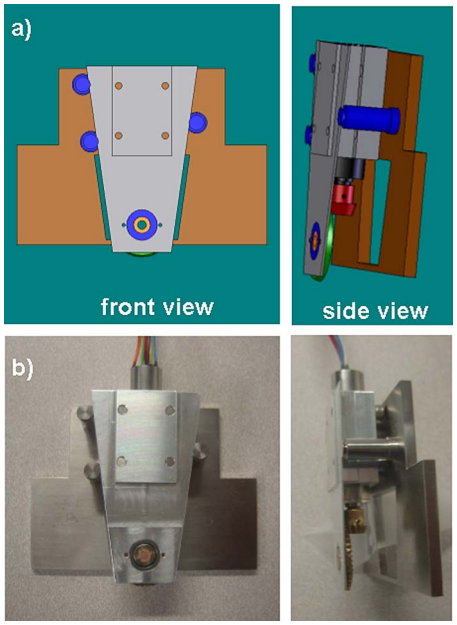

FIG. 2. (a) Design of the motorized azimuthal rotation sample holder [design and figure using 3D solid designer (Ref. 16)]. (b) Pictures of the device mounted in the three-pin kinematic mount.

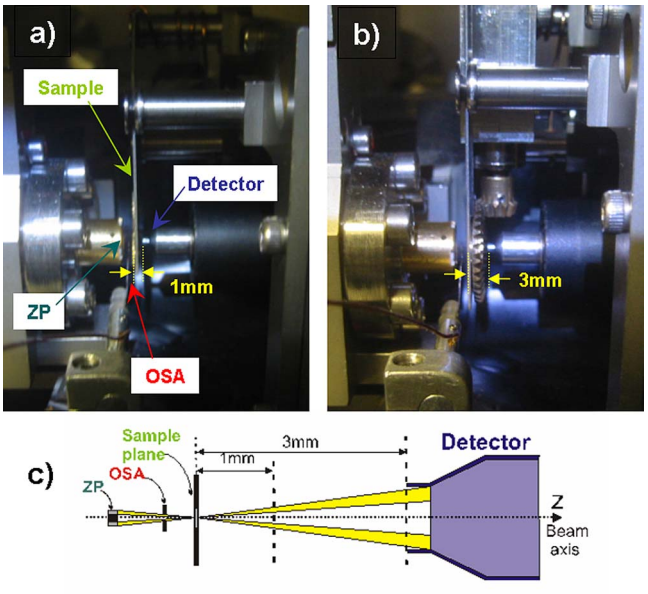

FIG. 3. (a) The manual azimuthal rotation sample holder mounted in STXM 5.3.2. (b) The motorized azimuthal rotation sample holder mounted in STXM 5.3.2. (c) Illustration of the x-ray beam divergence which leads to the requirement for the detector to be positioned such that its front is no more than 3 mm downstream of the focal point.

might take only 10 min. Recently, we have developed an *in situ* motorized azimuthal rotating sample holder (Fig. 2). Provision for *in situ* sample rotation with the device described in this article allows the sample orientation to be changed much more rapidly (<1 min). This facilitates more efficient use of beam time, which is important since both STXMs at the ALS are in very heavy demand. The device provides higher quality data, since, in the same time period, it can give more regular and more frequent sampling over a range of angles. It also allows positioning at specific angles such as 0°, 54°, and 90° between the *E* vector and a sample alignment vector. The device, its characterization and performance, and some results obtained from a spider silk fiber—a partially oriented biopolymer—are described. In addition, this article describes a new development in the analysis of this type of data, which provides maps of the orientation vector as well as the magnitude derived from NEXAFS linear dichroism.

II. DESIGN AND CONSTRUCTION

The geometry of STXM, especially in the soft x-ray region where the focal length is very small, placed severe constraints on the design of the *in situ* motorized azimuthal rotator holder. In the design process, the device was required to have the same form factor as the normal sample holder plate, since this provides kinematic mounting which achieves ~10 μm reproducibility of positioning (see Fig. 1 for a view of the pins which provide the positional registry[15]). In addition, it should not come into contact with any other microscope parts or their motion stages. In particular, it has to avoid contact with the order sorting aperture (OSA), which is a 55 μm laser-drilled aperture in a piece of shim metal sitting at 200–300 μm upstream from the sample. Due to a very small angular acceptance of the detector (limited by a

600 μm acceptance aperture) and the rapid divergence of the x rays after they pass through the sample, the front of the detector has to be positioned no more than 3 mm downstream from the sample. Finally, due to the limited capacity of the fast scan piezo stage, the total mass had to be less than 100 g. These challenges, as well as the availability of specific miniature gears and bushings, lead to the final design, which is shown as a virtual view of the full device [constructed using SOLIDWORKS (Ref. 16)] in Fig. 2(a) and as a photograph in Fig. 2(b).

The commercial pieces used to construct the device included a brass bevel gear set (teeth 36, 48 pitch 3:1 ratio),[17] a metric flanged bearing (shaft diameter=5 mm),[18] and an 8 mm miniature stepper motor with a 64:1 ratio gear head and a built-in encoder.[19] The body of the device was made of aluminum. The total weight including the motor is about 35 g. The stepper motor is controlled using one channel of a multichannel Newport EPS7000 motion controller/driver[20] (which is interfaced to the STXM control software) or with a stand alone external motor driver.[21]

A major challenge for this design was the very limited z extent allowed due to the requirement that the detector be placed no more than 3 mm downstream from the focal plane. Modifications to the commercial bevel gears were required. The detector acceptance depends on the beam divergence which is proportional to the x-ray energy. Figure 3(a) shows the manual rotator placed into the STXM chamber, while Fig. 3(b) shows the motorized rotator placed in the STXM chamber. The sketch, in Fig. 3(c), illustrates how the beam diverges along the z axis (first order diffracted light, in yellow). The dashed vertical lines in Fig. 3(c) indicate the position of the 600 μm diameter aperture at the front of the detector. Normally, the detector is positioned at the dashed line, ~1 mm behind the sample. When the 3 mm thick *in situ* azimuthal rotation device is used, the detector has to be moved 2 mm back from its nominal position, such that the front surface of the detector is 3 mm behind the focal plane. If the detector is moved any farther downstream, the outer part of the transmitted x rays is blocked by the body of the detector. The high spatial resolution component of the signal is at the outer edges of the x-ray beam, since this portion corresponds to diffraction from the outer zones of the zone plate which are known to determine the spatial resolution.[22]

TABLE I. Measured deviations in angular position.

Requested angle	Angular error (measured—requested)		
	Newport controller (without encoder)		External controller (with encoder)
	Sample A	Sample B	Angular error
0	−1.5	−0.5	0.3
15	0.6	−0.1	0.0
30	−2.9	−4.6	−0.4
54	0.8	−4.7	0.3
72	−3.2	−2.5	0.6
90	−2.9	−0.2	0.5
Average error	−1.5(12)	−2.1(22)	+0.2(2)

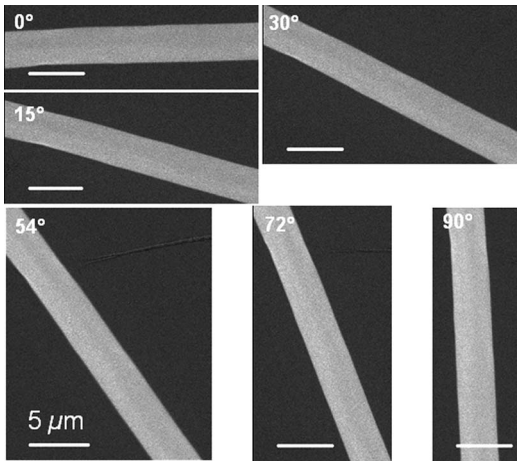

FIG. 4. OD(π^*) images at six different angles of a longitudinal section of a *N. clavipes* dragline spider silk fiber measured using the *in situ* azimuthal rotation device. The OD(π^*) images were constructed from images acquired at three energies in order to isolate the signal corresponding to the C 1s $\rightarrow \pi^*_{\text{amide}}$ transition which relates to protein orientation [OD(π^*) =OD(288.2)−(OD(287.4)+OD(289.0))/2].

Thus, placing the detector too far behind the sample degrades not only signal strength but also spatial resolution.

III. PERFORMANCE AND RESULTS

Table I displays results on the precision of the rotation when using the Newport ESP7000 controller. The angle of the sample was derived from the STXM image. The precision and accuracy using this controller was only 2°, even when the set position was consistently approached in a clockwise sense to minimize backlash error. This disappointing result is most likely due to the fact that the encoder signal provided by the Faulhaber motor is not compatible with the Newport ESP7000 controller, so the control of po-

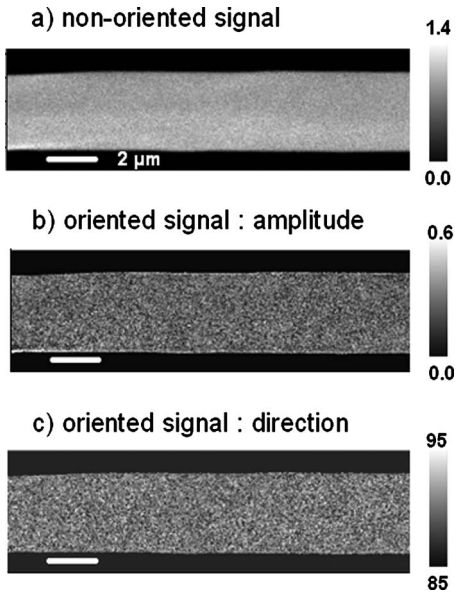

FIG. 5. Polarization mapping analysis of the dichroic signal from rotated and aligned versions of the images displayed in Fig. 4. (a) Map of the nonoriented signal. (b) Map of the magnitude of the dichroic signal. (c) Map of the direction of maximum intensity of the dichroic signal (angle relative to the fiber axis). See text for further details.

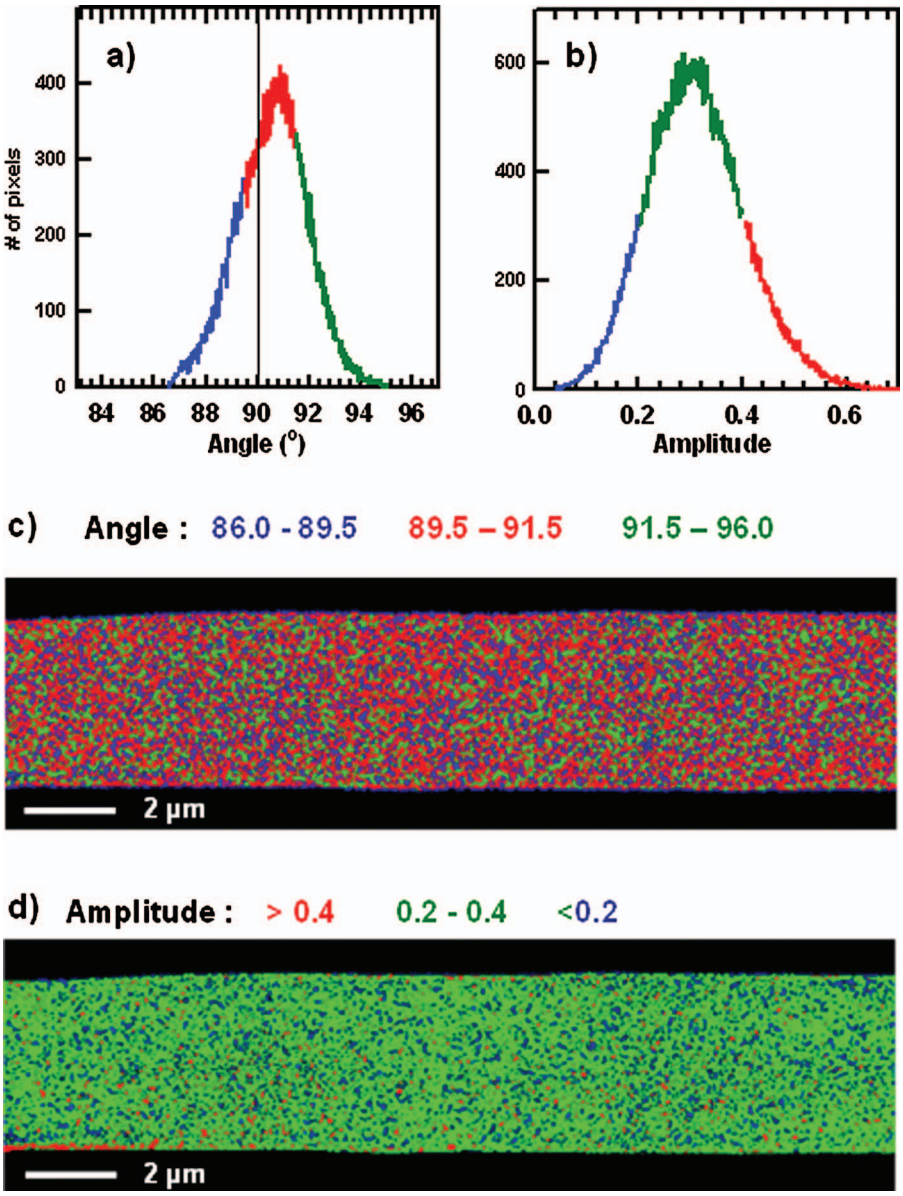

FIG. 6. (Color) (a) Histogram of the direction of maximum intensity of the dichroic signal. (b) Histogram of the magnitude of the dichroic signal. (c) Colored version of the map of the direction of maximum intensity of the dichroic signal using the angle ranges indicated in Fig. 6(a) for red, green, and blue. (d) Colored version of the map of the magnitude of the dichroic signal using the amplitude ranges indicated in Fig. 6(b) for red, green, and blue. These plots are based on the data displayed as component maps in Fig. 5.

sition was based only on counting stepper motor pulses rather than encoder feedback. When an external stepper motor controller which uses the encoder signal and antibacklash operation was used, the angular positioning was both precise and accurate to within 0.2°, as shown in Table I.

Figure 4 displays an example of the type of angle dependent data measured with the *in situ* motorized azimuthal rotation sample holder for a *N. clavipes* spider silk sample. The data for Fig. 4 was obtained at a rate of 40 min per angle, since a very fine point spacing (30 nm pixels), a relatively large sample area ($18 \times 15\ \mu m^2$), and a long dwell/pixel (2.2 ms) was used. In contrast, the recording of the same data using the nonmotorized approach is estimated to take about 80 min per angle. Clearly, the new device decreases the time for changing from one angle to another. The improved efficiency can be used to enhance results in a number of ways. More angles can be recorded with similar data sampling; more finely sampled images can be acquired on a given sample area for improved precision; a larger sample area can be measured, or more samples can be measured, using a similar measurement protocol.

We have recently shown that it is possible to use data like those presented in Fig. 4 to quantitatively map the level of orientation of the carbonyl bonds of the polypeptide chains at high spatial resolution in *B. mori* cocoon silk[6] and *N. clavipes* spider dragline silk.[7] In these studies, maps of the order parameter $\langle P_2 \rangle$ were calculated from the ratio of the maps obtained with the *E* vector of the x-ray beam at 0° and 90° from the fiber axis. The results obtained have shown that the carbonyl groups of the peptide bonds are predominantly oriented perpendicular to the fiber axis, in good agreement with the structural model of the oriented β sheets found in silk fibers. Although this approach gives valuable quantitative information on the average orientation of the peptide groups, it does not provide any information on the width and shape of the orientation distribution. Here, we present a new approach to the analysis of angle-dependent STXM data,

which has recently been implemented in the AXIS2000 software package.[23]

As with the previous analysis,[6,7] sets of three images recorded at each angle are first processed to isolate the π^*_{amide} signal $[\text{OD}(\pi^*)=\text{OD}(288.2)-(\text{OD}(287.4)+\text{OD}(289.0\ \text{eV}))/2]$. The $\text{OD}(\pi^*)$ images (Fig. 4) are then carefully rotated to the same orientation (horizontal) and aligned precisely (0.1°). They are then combined in a three-dimensional data array (a polarization image sequence, analogous to a photon energy dependent stack[24]). In the new approach, the dichroic signal at each pixel (indices j and k) $I_{jk}(\theta)$ is fitted using the following equation:

$$I_{jk}(\theta) = C_{jk} + A_{jk}\cos^2(\theta - B_{jk}), \quad (1)$$

where C_{jk} is a constant (signal from nonoriented proteins at the jk pixel), A_{jk} is the amplitude of the dichroic signal, and B_{jk} is the angle of maximum intensity. The values from the fit to the angle-dependent signal at each (jk) pixel are then assembled into maps of the nonoriented signal (C), the amplitude of the dichroic signal (A), and the direction of orientation of the dichroic signal (B). We have found that it is important to check that the fit has converged, by varying the tolerance, maximum number of iterations, and initial values of the A, B, and C parameters. The results presented here are from a converged fit.

Figure 5 displays the maps of the A, B, and C parameters. There is structure in the map of the nonoriented C $1s \rightarrow \pi^*_{\text{amide}}$ signal (C). In particular, the lower part is ~10% more intense than the upper part of the fiber. This is attributed to a thickness or density variation, possibly associated with microtoming. The map of the amplitude (A) of the dichroic signal does not show this variation, consistent with the above explanation. Instead, it shows a structure with a very fine scale. This signal was reported elsewhere,[7] but was derived with different data processing. Relative to the previous analysis, the map of the direction (angle relative to the E vector) of the maximum intensity of the dichroic signal (B), shown in Fig. 5(c), provides new information. A histogram of the map for the B_{jk} parameter (the angle of the maximum of the dichroic signal) is presented in Figure 6(a). The angle of the maximum of the dichroic signal (relative to the fiber axis) is predominantly perpendicular to the fiber axis but the mean angle is 91° and the distribution is skewed slightly to lower angles. The slight shift from the expected angle of 90° might indicate that the carbonyl groups in the highly aligned portions of the protein are rotated slightly in a particular direction, for example, towards or away from the front of the fiber as it is being spun (we do not know which is the front or the back end of the fiber in this case). However, the edges of the fiber are not perfectly parallel so this shift may simply be an offset between our visual selection of the fiber axis and the true fiber axis. Figure 6(b) shows the histogram of the dichroic amplitudes (A), while Figs. 6(c) and 6(d) present color coded maps in which the pixels of the fiber are colored based on the specified ranges of values of the direction angle and amplitude distributions. Further insight can be obtained by using the amplitudes of the dichroic signal to partition the maps of B, the direction (angle) of maximum dichroic intensity. The results of this analysis are presented in Fig. 7(a)

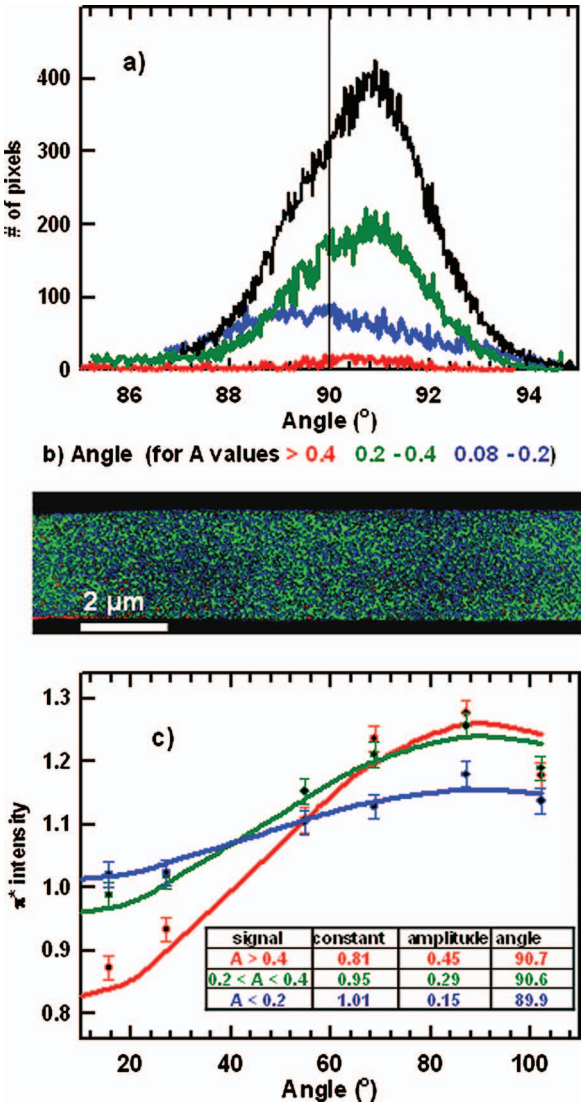

FIG. 7. (Color) (a) Histogram of the direction of maximum intensity of the dichroic signal, partitioned according to the amplitude of the dichroic signal. Red—high amplitude of dichroic signal (>0.4); green—intermediate amplitude of dichroic signal (0.2–0.4); blue—low amplitude of dichroic signal (<0.2). (b) Colored map of the direction of maximum intensity of the dichroic signal using the signals indicated in Fig. 7(a) for red, green, and blue. The values of direction angles in each amplitude range are mapped to the 0–255 scale for each color. (c) Extracted signal and curve fit to Eq. (1), for data extracted from pixels with amplitude values >0.4 (red), $0.2<A<0.4$ (green), and <0.2 (blue). The insert table summarizes the A, B, and C parameters derived from the fits to Eq. (1).

which plots the histogram of the direction angles (B) for those pixels with dichroic amplitudes (A) in the ranges of high dichroic signal $(A>0.4$, plotted in red), intermediate dichroic signal $(0.2<A<0.4$, plotted in green), and low dichroic signal $(A<0.2$, plotted in blue). Here one sees that the pixels with high dichroic amplitude have a mean angle of 90.6°, well aligned with the expected 90° orientation, while those with low and intermediate dichroic amplitude span a wider range of direction angles with the pixels of low dichroic amplitude skewed to lower angle and the pixels with intermediate dichroic amplitudes skewed to slightly higher angle. A colorized map of these categorized signals is presented in Fig. 7(b), while Fig. 7(c) shows fits using Eq. (1) to the signals extracted from pixels with amplitude values >0.4

(red), $0.2 < A < 0.4$ (green), and < 0.2 (blue) to illustrate the differences in the dichroic signals extracted by partitioning based on dichroic amplitudes.

This approach to analyzing the dichroic signals using partitioning and colorization based on histograms is similar to but extends that presented elsewhere for the distributions of $\langle P_2 \rangle$ values.[7] It is a powerful way to examine the spatial distribution of alignment, which is believed to be a controlling factor in the mechanical properties of silks. This new approach to the analysis of dichroic STXM data will be used to compare silks from different species, different types of silk from the same species, and silks pulled under controlled conditions at variable silking speeds. Such systematic studies should assist ongoing efforts to develop biosynthetic silk derivatives.

IV. SUMMARY

A motorized azimuthal rotation sample holder was designed, constructed, and used to perform linear dichroism measurements by STXM at the ALS beamline 5.3.2. The device weighs ~35 g and positions the sample orientation with a rotational accuracy of 0.2°. This sample holder is also being used at ALS beamline 11.0.2 and at the Canadian Light Source beamline 10ID1 (Ref. 25) to verify the linear polarization of an Apple-type EPU line, using highly oriented samples with well known orientation directions. An improved approach of the analysis of the linear dichroic signals was presented and illustrated with azimuthally dependent signals from a *N. clavipes* dragline spider silk sample.

ACKNOWLEDGMENTS

This research was supported by Natural Science and Engineering Research Council (NSERC, Canada), Canada Foundation for Innovation, and the Canada Research Chair programs. The authors thank Dr. Gary Mitchell for providing the manual rotational sample plate used in the STXM 5.3.2. measurements, Dr. Göran Johansson for assistance with implementing the motorized system, and Marcia Reid for expert sample preparation. Construction and operation of the STXM 5.3.2 microscope is supported by NSF DMR-9975694, DOE DE-FG02-98ER45737, Dow Chemical, NSERC, and the Canada Foundation for Innovation. The authors thank David Kilcoyne for his contribution to developing and maintaining the instrument. The Advanced Light Source is supported by the Director, Office of Energy Research, Office of Basic Energy Sciences, Materials Sciences Division of the U.S. Department of Energy, under Contract No. DE-AC03-76SF00098.

[1] H. Ade in *X-Ray Spectromicroscopy*, Experimental Methods in the Physical Sciences, edited by J. A. R. Samson and D. L. Ederer (Academic, New York, 1998), Vol. 32, pp. 225–256.
[2] H. Ade, S. G. Urquhart, in *Chemical Applications of Synchrotron Radiation*, edited by T. K. Sham (World Scientific, Singapore, 2002), pp. 285–355.
[3] J. Stöhr, *NEXAFS Spectroscopy*, Springer Tracts in Surface Science Vol. 25 (Springer, Berlin, 1992).
[4] A. P. Smith and H. Ade, Appl. Phys. Lett. **69**, 3833 (1996).
[5] A. P. Smith, C. Bai, H. Ade, R. J. Spontak, C. M. Balik, and C. C. Koch, Macromol. Rapid Commun. **19**, 557 (1998).
[6] D. Hernández-Cruz, M.-E. Rousseau, M. M. West, M. Pézolet, and A. P. Hitchcock, Biomacromolecules **7**, 836 (2006).
[7] M.-E. Rousseau, D. Hernández-Cruz, M. M. West, A. P. Hitchcock, and M. Pézolet, J. Am. Chem. Soc. (in press).
[8] C. Riekel, M. Burghammer, and M. Müller, J. Appl. Crystallogr. **33**, 421 (2000).
[9] C. Riekel, B. Madsen, D. P. Knight, and F. Vollrath, Biomacromolecules **1**, 622 (2000).
[10] C. Riekel and F. Vollrath, Int. J. Biol. Macromol. **29**, 203 (2001).
[11] L. F. Drummy, D. M. Phillips, H. Koerner, R. A. Vaia, B. L. Farmer, and R. R. Naik, Microsc. Microanal. **11**, 1268 (2005).
[12] H. Bluhm *et al.*, J. Electron Spectrosc. Relat. Phenom. **150**, 86 (2005).
[13] A. T. Young, E. Arenholz, S. Marks, R. Schlueter, C. Steier, H. A. Padmore, A. P. Hitchcock, and D. G. Castner, J. Synchrotron Radiat. **9**, 270 (2002).
[14] T. Warwick *et al.*, J. Synchrotron Radiat. **9**, 254 (2002).
[15] A. L. D. Kilcoyne *et al.*, J. Synchrotron Radiat. **10**, 125 (2003).
[16] SOLIDWORKS, a three-dimensional (3D) mechanical design and 3D computer aided design (CAD) software, http://www.solidworks.com/
[17] Small parts Inc., http://www.smallparts.com/
[18] McMaster Carr, http://www.mcmaster.com/
[19] Faulhaber, http://www.faulhaber-group.com/
[20] Newport: Universal Motion Controller/driver, ESP 7000, http://www.newport.com/ESP7000-Universal-High-Performance-Motion-Controll/140198/1033/catalog.aspx
[21] JOVA Solutions, http://www.jovasolutions.com/hardware/tims0200_overview.htm
[22] D. Attwood, *Soft X-Rays and Extreme Ultraviolet Radiation* (Cambridge University Press, Cambridge, 1999).
[23] AXIS2000 is a freeware program written in Interactive Data Language (IDL) and available for noncommercial use from http://unicorn.mcmaster.ca/aXis2000.html
[24] C. Jacobsen, S. Wirick, G. Flynn, and C. Zimba, J. Microsc. **197**, 173 (2000).
[25] K. Kaznacheyev, I. Blomqvist, E. Hallin, S. Urquhart, D. Loken, T. Tylisczak, T. Warwick, and A. P. Hitchcock, AIP Conf. Proc. **705**, 1303 (2004).